Polymer 177 (2019) 43–48

Contents lists available at ScienceDirect

Polymer

journal homepage: www.elsevier.com/locate/polymer

Internal structure and mechanical property of an anisotropic hydrogel with electrostatic repulsion between nanosheets

Koki Sano[a,b], Naoki Igarashi[a,b], Yuka Onuma Arazoe[a], Yasuhiro Ishida[b,*], Yasuo Ebina[c], Takayoshi Sasaki[c], Takaaki Hikima[d], Takuzo Aida[a,b,**]

[a] Department of Chemistry and Biotechnology, School of Engineering, The University of Tokyo, 7-3-1 Hongo, Bunkyo-ku, Tokyo, 113-8656, Japan
[b] RIKEN Center for Emergent Matter Science, 2-1 Hirosawa, Wako, Saitama, 351-0198, Japan
[c] National Institute for Materials Science, International Center for Materials Nanoarchitectonics, 1-1 Namiki, Tsukuba, Ibaraki, 305-0044, Japan
[d] RIKEN SPring-8 Center, 1-1-1 Kouto, Sayo, Hyogo, 679-5198, Japan

HIGHLIGHTS

- Effects of the electrostatic repulsion on the anisotropic hydrogel were systematically studied.
- It was proved that the nanosheets in the hydrogel under the deionized state adopt a monodomain structure.
- The enhancement of the electrostatic repulsion largely increased mechanical anisotropy of the hydrogel.

ARTICLE INFO

Keywords:
Anisotropic hydrogel
Anisotropic mechanical property
Electrostatic repulsion
Inorganic nanosheets

ABSTRACT

We recently developed a mechanically anisotropic hydrogel with a large internal electrostatic repulsion. The hydrogel is embedded with negatively charged titanate nanosheets that are cofacially oriented by a magnetic field. Because of the anisotropic electrostatic repulsion between the nanosheets, this hydrogel exhibits a large elastic modulus when compressed orthogonal to the nanosheet plane. In this paper, we systematically investigate how the intensity of the electrostatic repulsion affects the internal structure and mechanical property of this anisotropic hydrogel, where the free-ion concentration in the hydrogel medium was the key parameter for moderating the electrostatic repulsion due to its screening effect. With gradually changing the free-ion concentration in the hydrogel, nanoscopic arrangement and mesoscopic domain structure of the nanosheets were characterized by two-dimensional small-angle X-ray scattering (2D SAXS) and confocal laser scanning microscopy (CLSM), respectively. Furthermore, an anisotropic mechanical property of the hydrogel was evaluated by compression test. These results reveal that extensive deionization of the hydrogel medium and the resultant maximization of the electrostatic repulsion induces the nanosheets to adopt a monodomain lamellar structure that occupies the whole space of the hydrogel, thereby enhancing the mechanical anisotropy of the hydrogel.

1. Introduction

Hydrogels are an important class of soft materials composed of three-dimensionally (3D) crosslinked networks that can accommodate an abundance of water [1–3]. In general, hydrogels are similar to biological tissues and biocompatible because of their water-rich flexible structures. Therefore, they have been expected to find various applications in biomedical fields [4–6]. However, from a structural point of view, typical synthetic hydrogels are substantially different from biological systems. The 3D networks of synthetic hydrogels are generally isotropic, whereas those of most biological tissues, such as muscles [7], skin [8], and articular cartilage [9,10], are geometrically anisotropic up to macroscopic length scales. These anisotropic structures play essential roles in specific biological functions, including actuation, mass transport, surface lubrication, and mechanical anisotropy. Inspired by these sophisticated systems, a variety of anisotropic hydrogels have been developed [11,12]. The design strategy for anisotropic hydrogels has mainly relied on the attractive interactions between anisotropically oriented building blocks, such as nanofillers and polymer networks [11,12]. In contrast, articular cartilage, for example, utilizes a large

* Corresponding author. RIKEN Center for Emergent Matter Science, 2-1 Hirosawa, Wako, Saitama, 351-0198, Japan.
** Corresponding author. RIKEN Center for Emergent Matter Science, 2-1 Hirosawa, Wako, Saitama, 351-0198, Japan.
E-mail addresses: y-ishida@riken.jp (Y. Ishida), aida@macro.t.u-tokyo.ac.jp (T. Aida).

https://doi.org/10.1016/j.polymer.2019.05.064
Received 28 March 2019; Received in revised form 18 May 2019; Accepted 25 May 2019
Available online 28 May 2019
0032-3861/

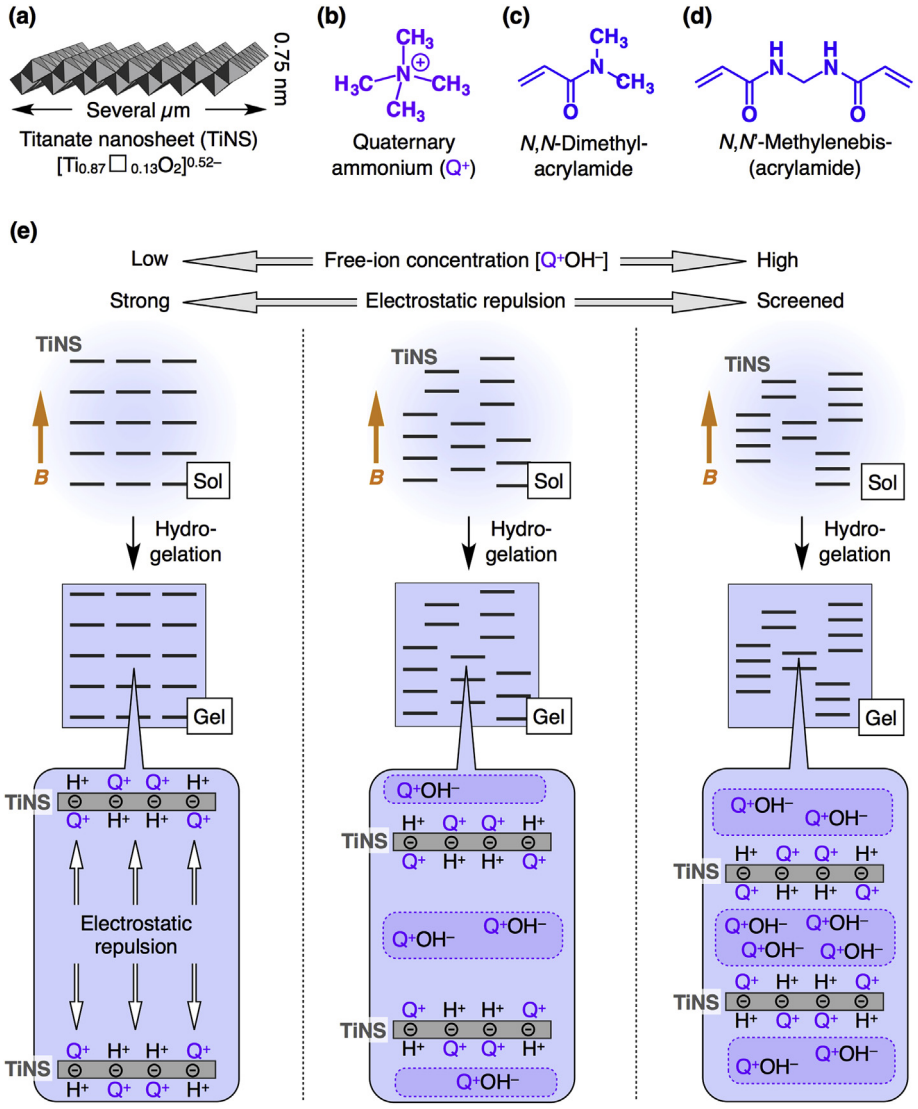

Fig. 1. (a–d) Schematic illustration of a negatively charged titanate nanosheet (a) and chemical structures of its quaternary ammonium counterion (Q^+; b), a monomer (*N*,*N*-dimethylacrylamide; c), and a crosslinker (*N*,*N*′-methylenebis (acrylamide); d). In (a), □ indicates a vacant site. (e) Synthesis of anisotropic hydrogels using aqueous dispersions of TiNSs with various free-ion concentrations ([Q^+OH^-]). *B* indicates a magnetic field vector.

anisotropic electrostatic repulsion between negatively charged polymers to realize both high load bearing and smooth mechanical motion in joints [9,10].

Inspired by articular cartilage, we recently developed a novel anisotropic hydrogel with internal electrostatic repulsion [13]. The key unit for generating the electrostatic repulsion is a unilamellar titanate (IV) nanosheet (TiNS; Fig. 1a) [14,15], which is characterized by the high density of negative charges ($1.5\,C\,m^{-2}$) and high aspect ratio ($\sim 10^4$). When an aqueous dispersion of TiNSs is placed in a strong magnetic field, TiNSs align orthogonal to the applied magnetic flux lines, so that they adopt a cofacial geometry (Fig. 1e, upper) [13,16]. As a result, an anisotropic electrostatic repulsion emerges between the TiNSs. This magneto-induced anisotropic structure can be fixed by the in-situ polymerization of acrylic monomers (Fig. 1e). Owing to the embedded anisotropic electrostatics, the resultant hydrogel exhibits anisotropic mechanical properties that are reminiscent of articular cartilage [13]; the hydrogel easily deforms when a shear force is applied parallel to the TiNS plane but is highly resistant to a compressive force applied orthogonal to the plane. As an extension of this design concept, we developed an unprecedented type of hydrogel actuator, in which the anisotropic electrostatic repulsion between cofacially aligned TiNSs can be thermally modulated [16].

After these works, we serendipitously found that the electrostatic repulsion between as-prepared TiNSs was largely attenuated by excess amount of free ions (tetramethylammonium hydroxide, Q^+OH^-; Fig. 1b) that were used for the exfoliation of TiNSs [17]. As expected, by removing such free ions, we successfully obtained much more anisotropic hydrogels with more enhanced electrostatic repulsion [18]. However, it has not been systematically studied how the intensity of the electrostatic repulsion affects the internal structure and mechanical property of the anisotropic hydrogel. In the present work, we investigated the nanoscopic arrangement of TiNSs, their mesoscopic domain structure, and mechanical property of the anisotropic hydrogel by changing the free-ion concentration ([Q^+OH^-]), because the strength of electrostatic repulsion is supposed to be highly influenced by [Q^+OH^-], according to the Derjaguin-Landau-Verwey-Overbeek (DLVO) theory [19].

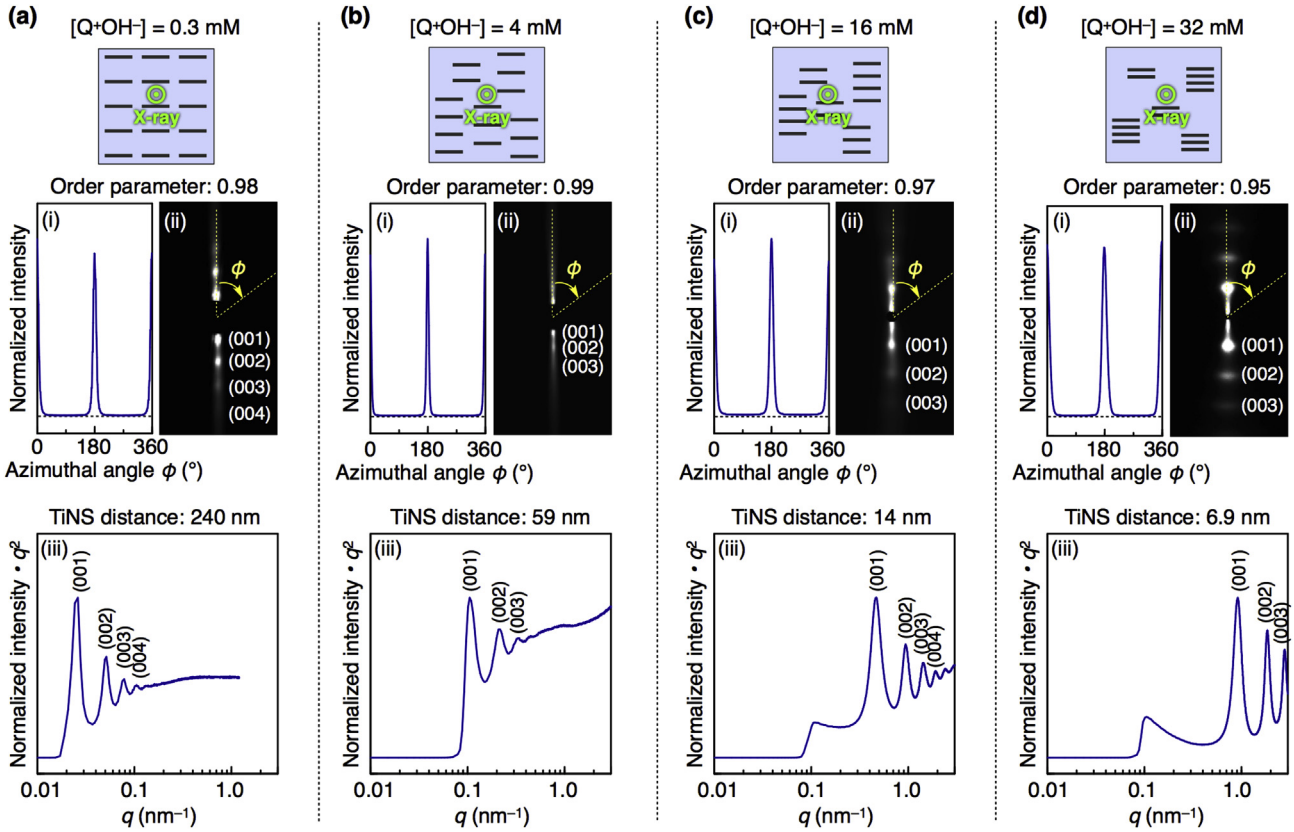

Fig. 2. (a–d) 2D SAXS images upon parallel X-ray irradiation to the cofacially oriented TiNS plane (ii), the corresponding azimuthal angle plots (i) and 1D profiles (iii) of the anisotropic hydrogels ([TiNS] = 0.8 wt%) with various free-ion concentrations: $[Q^+OH^-]$ = 0.3 (a), 4 (b), 16 (c), and 32 mM (d).

2. Experimental section

2.1. Materials

Titanate nanosheets (TiNSs) were prepared according to the literature method [15]. *N,N*-Dimethylacrylamide (Fig. 1c, Tokyo Chemical Industry) was deionized by using a mixed-bed ion exchange resin and then passed through an alumina column for removing 4-methoxyphenol inhibitor. 2,2-Diethoxyacetophenone (Wako Pure Chemical Industries) was deionized by using a mixed-bed ion exchange resin. *N,N′*-Methylenebis (acrylamide) (Figs. 1d) and 15% tetramethylammonium hydroxide aqueous solution (Wako Pure Chemicals Industries) were used as received. Water was obtained from a Millipore model Milli-Q integral water purification system.

2.2. Preparation of TiNS dispersions with various free-ion concentrations [17]

An aqueous dispersion (40 mL) of TiNSs (0.4 wt%), as synthesized by the literature method (Fig. S1, i) [15], was centrifuged at a centrifugal force of 20,000*g* for 1 h. The supernatant (35 mL) was removed from the centrifugation tube, and the residue was redispersed by adding deionized water. With repeating the similar centrifugation and redispersion more than eight times, the free-ion concentration ($[Q^+OH^-]$) in the TiNS dispersion (0.4 wt%) was reduced from ~10 to 0.1 mM, and further deionization was not possible even when the similar processes were repeated (Fig. S1, ii). The free-ion concentrations ($[Q^+OH^-]$) were estimated by conductivity measurements using a Horiba model DS-71E conductivity meter. To the fully deionized TiNS dispersion thus obtained ([TiNS] = 0.8 wt%, $[Q^+OH^-]$ = 0.3 mM), calculated amounts of tetramethylammonium hydroxide (Q^+OH^-) were added for preparing the TiNS dispersions with various free-ion concentrations ($[Q^+OH^-]$ = 0.3–49 mM).

2.3. Preparation of anisotropic hydrogels [13,16,18]

N,N-Dimethylacrylamide as a monomer (6.0 wt%; Fig. 1c), *N,N′*-methylenebis (acrylamide) (0.06 wt%; Fig. 1d) as a crosslinker, and 2,2-diethoxyacetophenone (0.08 wt%) as a photoinitiator were added to an aqueous dispersion of TiNSs so that final [TiNS] became 0.8 or 0.4 wt%. The resultant mixture (1.2 mL) in a rectangular-shaped polystyrene cuvette (10 mm × 10 mm) was placed in the bore of a 10-T superconducting magnet (a JASTEC model JMTD-10T100) at 20 °C for 30 min to allow TiNSs to align orthogonal to the magnetic flux lines (Fig. 1d, upper). The dispersion was then exposed to a 500-W high-pressure mercury arc light (an USHIO model OPM2-502H) in the magnetic flux for 30 min to initiate the in-situ radical polymerization, affording an anisotropic hydrogel (Fig. 1d).

2.4. Synchrotron small-angle X-ray scattering analysis

Two-dimensional small-angle X-ray scattering (2D SAXS) measurements of the hydrogels were carried out at BL45XU in the SPring-8 synchrotron radiation facility (Hyogo, Japan) [20] using a Dectris model PILATUS3X 2 M detector or a Rigaku model R-AXIS IV++ imaging plate area detector. The scattering vector ($q = 4\pi\sin\theta/\lambda$) and position of an incident X-ray beam on the detector were calibrated using several orders of layer reflections from silver behenate (d = 58.380 Å), where 2θ and λ are the scattering angle and wavelength of an incident X-ray beam (1.0 or 1.7 Å), respectively. The sample-to-detector distance was 2.5 or 3.5 m. The anisotropic hydrogels ([TiNS] = 0.8 wt%) with various free-ion concentrations ($[Q^+OH^-]$ = 0.3–32 mM) were sliced into ~1 mm-thick films so that the sliced plane was orthogonal to the nanosheet plane. Then, the X-ray

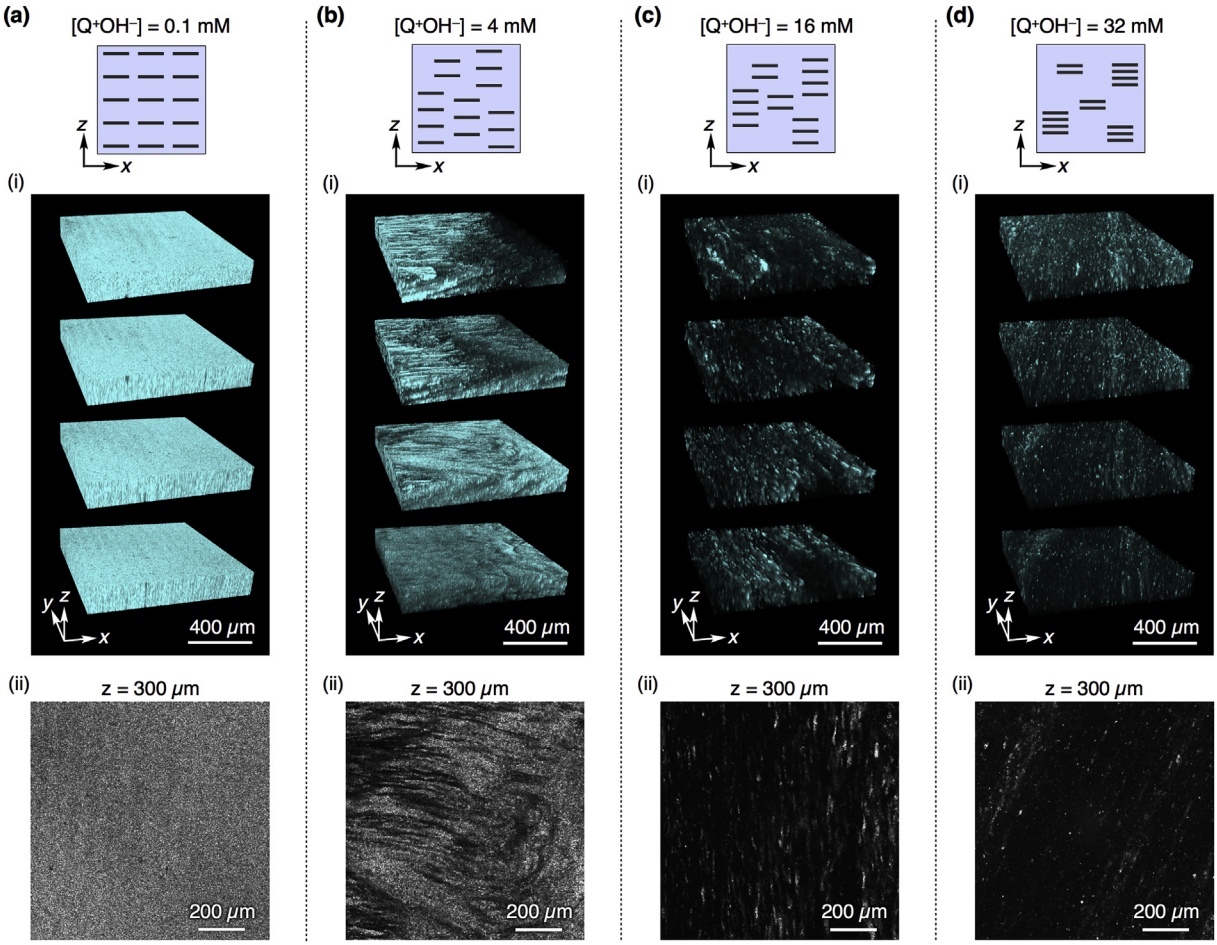

Fig. 3. (a–d) Sliced layers of reconstituted 3D CLSM images at various height (z = 0–600 μm; i) and representative cross-sectional 2D CLSM images (z = 300 μm; ii) of the anisotropic hydrogels ([TiNS] = 0.4 wt%) with various free-ion concentrations: $[Q^+OH^-]$ = 0.1 (a), 4 (b), 16 (c), and 32 mM (d).

beam was irradiated orthogonal to the sliced plane of the hydrogel films, affording 2D SAXS images. The obtained 2D images were integrated along the Debye–Scherrer ring by using Fit2D software [21], affording the corresponding 1D SAXS profiles. The scattering intensity-azimuthal angle plots were obtained from the scattering of the (002) face in the 2D SAXS images by using Fit2D software [21], and the order parameters were calculated according to the reported method [13,22].

2.5. Confocal laser scanning microscopy analysis

Confocal laser scanning microscopy (CLSM) analysis was performed at 25 °C on a Leica TCS SP8 confocal microscope system with a reflection mode (laser wavelength = 488 nm). The anisotropic hydrogels ([TiNS] = 0.4 wt%) with various free-ion concentrations ($[Q^+OH^-]$ = 0.1–32 mM) were sliced into ~1 mm-thick films so that the sliced plane was parallel to the nanosheet plane. The laser beam was irradiated orthogonal to the sliced plane of the hydrogel films (from the z-axis), affording CLSM 2D images parallel to the xy-plane (1 mm × 1 mm). These 2D images were collected as a z-step size of 2 μm and reconstituted from z = 0–600 μm to provide 3D information of TiNS domain.

2.6. Mechanical property measurement of anisotropic hydrogels

Compression test of the anisotropic hydrogels ([TiNS] = 0.8 wt%) with various free-ion concentrations ($[Q^+OH^-]$ = 0.3–49 mM) were carried out at 25 °C by using a Shimadzu model EZ Test machine. A cube-shaped (10 mm × 10 mm × 10 mm) hydrogel sample was set under an upper plate connected to a 10-N load cell. Compressive stress was measured with applied compression strain from 0 to 40% at a constant compression rate of 20% min^{-1}. Elastic moduli were calculated as the average tangent at a strain of 20% in the stress-strain curves.

3. Results and discussion

3.1. Nanoscopic arrangement of TiNSs in anisotropic hydrogels

In order to investigate the effect of the electrostatic repulsion between TiNSs on the nanoscopic arrangement of TiNSs, we conducted 2D SAXS measurements of the anisotropic hydrogels ([TiNS] = 0.8 wt%) with various $[Q^+OH^-]$ (0.3–32 mM). The X-ray beam was irradiated parallel to the nanosheet plane in an anisotropic hydrogel, affording a 2D SAXS image with a linear array of multiple scattering peaks corresponding to the (001), (002), (003), … faces of the cofacial TiNS arrangement with a uniform plane-to-plane distance (Fig. 2a–d, ii). When $[Q^+OH^-]$ was decreased from 32 to 0.3 mM, the TiNS distance obtained from 1D SAXS profiles increased from 6.9 to 240 nm (Fig. 2a–d, iii). This tendency can be explained by the DLVO theory, where it suggests that the lowering $[Q^+OH^-]$ enhances the electrostatic repulsion between TiNSs, thereby increasing the TiNS distance [17,19]. Indeed, the Debye length of TiNSs, a characteristic parameter to explain the electrostatic repulsion, was calculated, which increased from 1.1 to 12 nm upon lowering $[Q^+OH^-]$ (Supplementary section 1). In contrast, the order parameter of TiNSs in the hydrogels, which is calculated from the scattering intensity-azimuthal angle plots [22], is more than 0.95

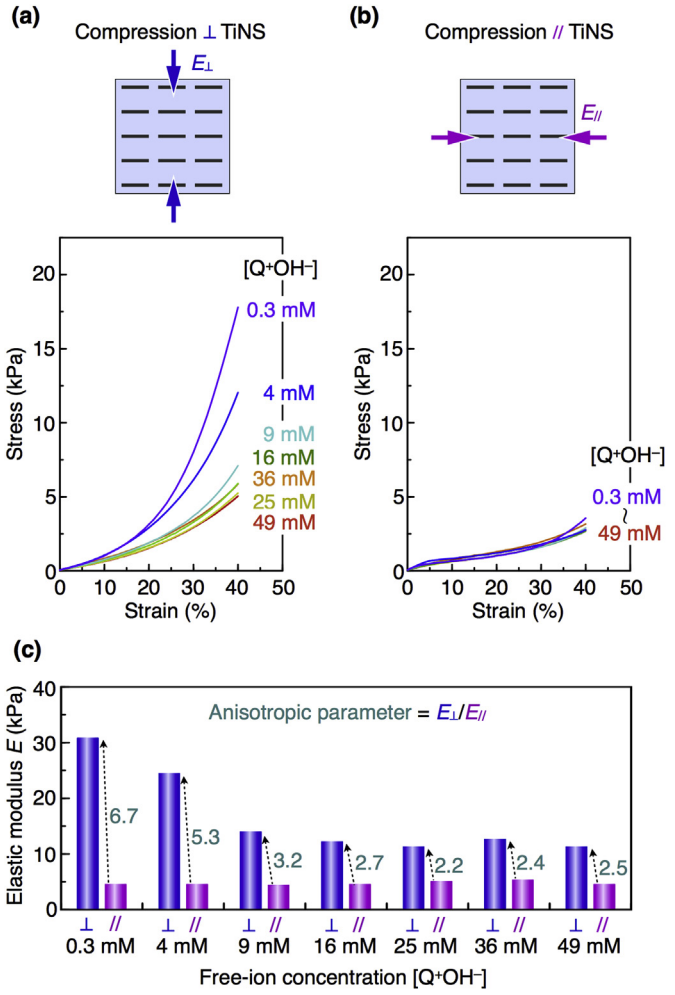

Fig. 4. (a,b) Strain–stress curves of the anisotropic hydrogels ([TiNS] = 0.8 wt %) with various free-ion concentrations ([Q^+OH^-] = 0.3–49 mM) upon orthogonal (a) and parallel (b) compressions to the cofacially oriented TiNS plane. (c) Elastic moduli (E) of the hydrogels at strain = 20% upon orthogonal ($E_\perp$; navy) and parallel ($E_{//}$; magenta) compressions with respect to the cofacially oriented TiNS plane. Anisotropic parameters ($E_\perp/E_{//}$) are shown in green. (For interpretation of the references to colour in this figure legend, the reader is referred to the Web version of this article.)

regardless of [Q^+OH^-], indicating a remarkably high orientational degree of TiNSs in the all hydrogels (Fig. 2a–d, i).

3.2. Mesoscopic domain structure of TiNSs in anisotropic hydrogels

In order to investigate the effect of the electrostatic repulsion between TiNSs on the mesoscopic domain structure of TiNSs, we conducted CLSM measurements of the anisotropic hydrogels ([TiNS] = 0.4 wt%) with various [Q^+OH^-] (0.1–32 mM). A reflection mode of CLSM selectively visualizes TiNSs that are oriented parallel to the *xy*-plane [23]. Because all TiNSs are oriented orthogonal to the *z*-axis in the anisotropic hydrogels as proved by the scattering intensity–azimuthal angle plots (Fig. 2a–d, i), the CLSM observation can provide 3D spatial distribution of the TiNS domain. Fig. 3d (i) shows the 3D structure (z = 0–600 μm) of the anisotropic hydrogel with [Q^+OH^-] = 32 mM, where the bright regions are the domains containing TiNSs, while the remaining dark regions are TiNS-free space. This multi-domain structure with a large free volume originates from the small TiNS distance (= 6.9 nm) because of the screened electrostatic repulsion between TiNSs, where the layered structure of TiNSs cannot fully occupy the whole volume of the hydrogel. Judging from the cross-sectional 2D image at z = 300 μm, the domain size of the layered structure of TiNSs was estimated as less than 10 μm (Fig. 3d, ii). When [Q^+OH^-] was decreased from 32 to 4 mM, the electrostatic repulsion between TiNSs was gradually enhanced to increase the TiNS distance, so that the volume fraction of bright regions in the hydrogels increased (Fig. 3b–d, i). Accordingly, the domain size of the layered structure of TiNSs became around 10–100 μm (Fig. 3b, ii). When [Q^+OH^-] was reduced to 0.1 mM, which was the most extensively deionized state realized by centrifugation, the 3D reconstituted image of the anisotropic hydrogel shows homogeneous brightness, indicating the formation of a monodomain structure of TiNSs without notable free volume (Fig. 3a, i and ii). These results reveal that by enhancing the electrostatic repulsion between TiNSs, the ratio and size of TiNS domain in the hydrogels gradually increase and the TiNS domain finally become a monodomain structure.

3.3. Compression test of anisotropic hydrogels

In order to investigate the effect of the electrostatic repulsion between TiNSs on the mechanical anisotropy of the hydrogels, we conducted their compression test by changing [Q^+OH^-] (0.3–49 mM) at a constant [TiNS] (0.8 wt%). As shown in the stress–strain curves in Fig. 4a and b, the mechanical properties of the hydrogels were dependent on the direction of compression. As we discussed in Supplementary section 2, the electrostatic repulsion between planes of TiNSs is much more dominant for mechanical property of the anisotropic hydrogels than that between edges of TiNSs (Fig. S2). Furthermore, [Q^+OH^-] is crucial for the mechanical anisotropy of the hydrogels. The hydrogel with the highest [Q^+OH^-] value (49 mM) showed an elastic modulus ($E_\perp$) of 11.3 kPa upon compression orthogonal to the TiNS plane (Fig. 4a). This value was 2.5 times larger than that measured with parallel compression ($E_{//}$ = 4.6 kPa; Fig. 4b). When [Q^+OH^-] was lowered from 49 mM to 0.3 mM, $E_\perp$ increased from 11.3 to 30.8 kPa (Fig. 4a), while $E_{//}$ changed only slightly (Fig. 4b). Consequently, the anisotropic parameter ($E_\perp/E_{//}$) dramatically increased from 2.5 to 6.7 with lowering [Q^+OH^-] (Fig. 4c). According to the previous section, the enhanced electrostatic repulsion between TiNSs increases the volume fraction of anisotropic TiNS domains and decreases that of isotropic hydrogel-matrix regions. These changes in mesoscopic domain structure of TiNSs possibly contribute to the enhancement of the mechanical anisotropy of the hydrogel.

4. Conclusions

In the present work, we systematically investigated the effect of the electrostatic repulsion between TiNSs on the internal structure and mechanical properties of the anisotropic hydrogel embedded with magnetically oriented TiNSs, with gradually changing free-ion concentration ([Q^+OH^-]) in the hydrogel. When [Q^+OH^-] was lowered, the electrostatic repulsion between TiNSs was enhanced to increase the TiNS distance, so that the layered structure of TiNSs became to occupy the whole volume of the anisotropic hydrogel. Consequently, the mechanical strength in the direction orthogonal to the TiNS plane was selectively reinforced to increase the mechanical anisotropy ($E_\perp/E_{//}$). We found that [Q^+OH^-] in the lower concentration region (0–10 mM) drastically affected the internal structure and mechanical property of the hydrogel. Therefore, the maximization of electrostatic repulsion between the nanosheets is critical to enhance the mechanical anisotropy of the hydrogel. This study provides deep insights of our anisotropic hydrogel containing anisotropic electrostatic repulsion between charged nanosheets and expands the scope of this materials design strategy using internal electrostatic repulsion.

Author information

The authors declare no competing financial interests.

Acknowledgements

This work was financially supported by a JSPS Grant-in-Aid for Scientific Research (S) (18H05260). We also acknowledge the ImPACT Program of Council for Science, Technology and Innovation (Cabinet Office, Government of Japan) and JST CREST Grant Number JPMJCR17N1, Japan. K.S. thanks JSPS for a Young Scientist Fellowship (16J08492), the Program for Leading Graduate Schools (MERIT), and the Hosokawa Powder Technology Foundation.

Appendix A. Supplementary data

Supplementary data to this article can be found online at https://doi.org/10.1016/j.polymer.2019.05.064.

References

[1] E.M. Ahmed, Hydrogel: preparation, characterization, and applications: a review, J. Adv. Res. 6 (2015) 105–121.
[2] Y.S. Zhang, A. Khademhosseini, Advances in engineering hydrogels, Science 356 (2017) eaaf3627.
[3] Q. Wang, J.L. Maynar, M. Yoshida, E. Lee, M. Lee, K. Okuro, K. Kinbara, T. Aida, High-water-content mouldable hydrogels by mixing clay and a dendritic molecular binder, Nature 463 (2010) 339–343.
[4] R. Langer, D.A. Tirrell, Designing materials for biology and medicine, Nature 428 (2004) 487–492.
[5] D. Seliktar, Designing cell-compatible hydrogels for biomedical applications, Science 336 (2012) 1124–1128.
[6] J. Li, D.J. Mooney, Designing hydrogels for controlled drug delivery, Nat. Rev. Mater. 1 (2016) 16071.
[7] A.F. Huxley, Muscular contraction, J. Physiol. 243 (1974) 1–43.
[8] E. Proksch, J.M. Brandner, J.-M. Jensen, The skin: an indispensable barrier, Exp. Dermatol. 17 (2008) 1063–1072.
[9] J.E. Scott, Elasticity in extracellular matrix 'shape modules' of tendon, cartilage, etc. A sliding proteoglycan-filament model, J. Physiol. 553 (2003) 335–343.
[10] D. Dean, L. Han, A.J. Grodzinsky, C. Ortiz, Compressive nanomechanics of opposing aggrecan macromolecules, J. Biomech. 39 (2006) 2555–2565.
[11] K. Sano, Y. Ishida, T. Aida, Synthesis of anisotropic hydrogels and their applications, Angew. Chem. Int. Ed. 57 (2018) 2532–2543.
[12] X. Le, W. Lu, J. Zhang, T. Chen, Recent progress in biomimetic anisotropic hydrogel actuators, Adv. Sci. 6 (2019) 1801584.
[13] M. Liu, Y. Ishida, Y. Ebina, T. Sasaki, T. Hikima, M. Takata, T. Aida, An anisotropic hydrogel with electrostatic repulsion between cofacially aligned nanosheets, Nature 517 (2015) 68–72.
[14] T. Sasaki, M. Watanabe, H. Hashizume, H. Yamada, H. Nakazawa, Macromolecule-like aspects for a colloidal suspension of an exfoliated titanate. Pairwise association of nanosheets and dynamic reassembling process initiated from it, J. Am. Chem. Soc. 118 (1996) 8329–8335.
[15] T. Tanaka, Y. Ebina, K. Takada, K. Kurashima, T. Sasaki, Oversized titania nanosheet crystallites derived from flux-grown layered titanate single crystals, Chem. Mater. 15 (2003) 3564–3568.
[16] Y.S. Kim, M. Liu, Y. Ishida, Y. Ebina, M. Osada, T. Sasaki, T. Hikima, M. Takata, T. Aida, Thermoresponsive actuation enabled by permittivity switching in an electrostatically anisotropic hydrogel, Nat. Mater. 14 (2015) 1002–1007.
[17] K. Sano, Y.S. Kim, Y. Ishida, Y. Ebina, T. Sasaki, T. Hikima, T. Aida, Photonic water dynamically responsive to external stimuli, Nat. Commun. 7 (2016) 12559.
[18] K. Sano, Y.O. Arazoe, Y. Ishida, Y. Ebina, M. Osada, T. Sasaki, T. Hikima, T. Aida, Extra-large mechanical anisotropy of a hydrogel with maximized electrostatic repulsion between cofacially aligned 2D electrolytes, Angew. Chem. Int. Ed. 57 (2018) 12508–12513.
[19] E.J.W. Verwey, J.T.G. Overbeek, Theory of the Stability of Lyophobic Colloids, Elsevier, 1948.
[20] T. Fujisawa, K. Inoue, T. Oka, H. Iwamoto, T. Uruga, T. Kumasaka, Y. Inoko, N. Yagi, M. Yamamoto, T. Ueki, Small-angle X-ray scattering station at the SPring-8 RIKEN beamline, J. Appl. Crystallogr. 33 (2000) 797–800.
[21] http://www.esrf.eu/computing/scientific/FIT2D/.
[22] S. Feng, X. Xiong, G. Zhang, N. Xia, Y. Chen, W. Wang, Hierarchical structure in oriented fibers of a dendronized polymer, Macromolecules 42 (2009) 281–287.
[23] A.A. Shah, B. Schultz, K.L. Kohlstedt, S.C. Glotzer, M.J. Solomon, Synthesis, assembly, and image analysis of spheroidal patchy particles, Langmuir 29 (2013) 4688–4696.